# EVALUATING THE IMPACTS OF URBANIZATION AND CLIMATE CHANGE ON STREAMFLOW BY COMPARING TWO NEIGHBORING BASINS IN TEXAS

A Thesis

by

MANQING SHAO

Submitted to the Office of Graduate and Professional Studies of
Texas A&M University
in partial fulfillment of the requirements for the degree of

MASTER OF SCIENCE

| | |
|---|---|
| Chair of Committee, | Huilin Gao |
| Committee Members, | Francisco Olivera |
| | Oliver W. Frauenfeld |
| Head of Department, | Robin Autenrieth |

December 2018

Major Subject: Civil Engineering

## ABSTRACT

Urbanization is an important driver of environmental problems. Severe urban flooding resulting from increased impervious area threatens resident security, household assets, and infrastructure integrity. However, the impacts of urbanization are generally intertwined with those from climate change, and cannot be separated easily. To systematically quantify the individual and combined impacts of urbanization and climate change on streamflow, we applied a paired catchments approach to two adjacent river basins in south-central Texas—the San Antonio River Basin (SARB) with fast urbanization and the Guadalupe River Basin (GRB) with no significant land cover change. The integrated, physically-based distributed hydrologic model — Distributed Hydrology Soil Vegetation Model — was set up with a 200-meter spatial resolution and 3-hourly time step to simulate the streamflow over both basins. The model is first calibrated (2000–2011) and validated (1966–2011). We then conduct the simulations using multiple scenarios: (1) the fixed 1970 land cover condition, (2) 1970–2011 time-varying land cover conditions, (3) continuous land cover maps with different extreme climate conditions, and (4) varied urban land cover maps with the scaled observed precipitations. The simulated streamflow results were then analyzed via the change point detection method and the elasticity test. The results show that (1) the change of monthly maximum streamflow (i.e., MMS) pattern is mainly contributed by the changing precipitation when there is little urbanization; (2) the abrupt change of MMS pattern for the SARB is mainly contributed by the urbanization in the San Antonio City area; and (3) the elasticity values of MMS to precipitation range from 1.5 to 3.0 for the SARB.

ACKNOWLEDGEMENTS

First, I would like to thank my committee chair, Dr. Gao Huilin. She is very patient and has a strong sense of responsibility. Dr. Gao always gives me suggestions, not only in my research, but also in my daily life. I also want to thank my committee members Dr. Francisco Olivera and Dr. Oliver Frauenfeld for their support throughout this research. Meanwhile, I appreciate the help from Gang Zhao and Dr. Kao Shih-Chieh. I am also very grateful for the help from my dear friends, including Zishuo Li, Yao Li, Cheryl Holmes and Yuxin Cui. I also want to thank Laura, Chris and all the department faculty and staff.

In addition, this study has also benefitted from the usage of Texas A&M High Performance Research Computing (http://hprc.tamu.edu). I would like to express my sincere gratitude to everyone and everything at Texas A&M University.

Finally, I appreciate my mother and father for their support and encouragement, contributions and selfless support.

## CONTRIBUTORS AND FUNDING SOURCES

This work was supervised by a thesis committee including Dr. Huilin Gao and Dr. Olivera of the Department of Civil Engineering, as well as Dr. Frauenfeld of the Department of Geography.

This work was funded by the National Science Foundation – CAREER Grant (CBET 1454297). The contents of this thesis are solely the responsibility of the author and do not necessarily represent the official views of Texas A&M University, Civil Engineering Department, nor the National Science Foundation.

TABLE OF CONTENTS

Page

Page

LIST OF FIGURES

Page

LIST OF TABLES

Page

# 1. INTRODUCTION

Globally, the urban population has gone through a five-fold increase from 1950 to 2014 (United Nations 2014). Specifically, over 80% of the US population resides in urban areas as of 2014. On the one hand, there is a robust relationship between urbanization and regional prosperity; on the other hand, urbanization augments the pressures put on the environment (Lee et al. 2003, Spence et al. 2008, Turok et al. 2013). One representative example of the environmental impacts of urbanization is the land cover changes from converting natural surfaces to artificial impervious areas (Ogden et al. 2011). The increased impervious area can significantly alter the natural hydrological processes, such as reducing infiltration, increasing the peak flow, and causing flows to peak earlier (DeFries and Eshleman 2004, Nowak and Greenfield 2012, Oni et al. 2015). Furthermore, it was found that with rapid global urbanization, more flooding happens in the urban areas while less occurs in rural areas (Wasko and Sharma 2017). Severe urban flooding threatens resident security, household assets, and infrastructure integrity (Jha et al. 2012). Therefore, it is critical for the government to develop sustainable water resources policies based on scientific research (Daniel et al. 2000, Winters et al. 2015, Cross et al. 2018, Lindner 2018).

The two main methods used to study the impacts of urbanization on streamflow are paired catchments analysis and hydrological modeling (Cuo et al. 2008). The method of paired catchments analysis originates from a study by Bates and Henry (1928), in which the influence of forest destruction was evaluated by comparing the streamflow of two contiguous river basins with similar climate, topography, and land cover types. After observing both basins for the first eight years without any land cover change, one of the

basins was denuded and the measurements were taken for the next eight years. By using the basin without deforestation as the "control object", the impact from land cover change on streamflow was assumed to be separated from climate change. Similarly, this idea can also be used to study the influence of urbanization on streamflow for river basins which are in similar climate conditions but in different stages of urbanization (Burns et al. 2005).

However, detection of the effects of urbanization (or any form of land cover change) on streamflow can be complicated by climate change. It has been found that annual precipitation across in the Contiguous United States (CONUS), has increased approximately 4% from 1901 to 2015 (Anderson et al. 2015). Yang et al. (2013) studied the observed precipitation and streamflow of two adjacent watersheds in Wisconsin – one included an urbanized region, and the other "reference" watershed was predominantly agricultural. They found that, in addition to urbanization, changes in regional precipitation climatology (due to large-scale climate change) also contribute to the changes in streamflow patterns (Yang et al. 2013). Hence, the approach of paired catchments analysis alone is inadequate to separate the impact of urbanization out from climate change on streamflow.

Hydrological modeling plays an increasingly important role in urban hydrology, as it can be utilized to separate the effects of urbanization and climate change. The most commonly used method is the one-factor-at-a-time (OFAT) approach, which compares the results from different scenarios by keeping all inputs/parameters the same except one (Chang et al. 2015; Natkhin et al. 2015). For example, Yang et al. (2017) applied the Soil and Water Assessment Tool (SWAT) to two watersheds of northeastern Tibetan Plateau

and conducted a series of model simulations using the same input data (e.g., meteorological data, DEM data) with the exception of different land cover maps.

While the OFAT approach is applicable to almost all hydrological models in theory, a key limitation is that highly spatially heterogeneous impervious cover cannot be accurately represented when a lumped model is used. Therefore, physically based distributed hydrological models have a distinct advantage of simulating highly heterogeneous land covers (JR and Tucci 1984; Wigmosta et.al. 1994). In distributed models, a basin is partitioned into many small grid cells such that different soil/land cover types can be taken into account to facilitate precise simulations (Brirhet and Benaabidate 2016). There are many previous studies which successfully applied the OFAT approach to various distributed hydrological models. For instance, the Urban Runoff Branching Structure Model (URBS-MO) was applied to two urban catchments with different land uses (Rodriguez et al. 2008). MIKE SHE was used to study the hydrologic response to five types of land use changes (i.e., forest, rice paddy, upland, urban, and grassland) for the Gyeongancheon watershed in Korea (Im et al. 2009). The Distributed Hydrology Soil Vegetation Model (DHSVM), with an urban module incorporated, was utilized to isolate the impacts of urbanization on a partially urbanized basin in Washington State (Cuo et al. 2008). In addition, Zhao et al. (2016) compared DHSVM simulations under different historical and projected land-cover maps in the San Antonio River Basin, and found that urbanization alone had a profound impact on the increased peak flows.

Even though the previous studies provided useful information about the impacts of urbanization on streamflow, the unavailability of continuous land cover maps (e.g.,

annual land cover maps) has hindered the accurate quantification of the urbanization impacts, and also has caused large uncertainties in the modeled results (Fletcher et.al. 2013). To conduct more reliable hydrological analysis, continuous land cover maps are essential (Zarezadeh and Giacomoni 2017). Although land use change models have been employed to create continuous land cover maps in some studies (Lin et al. 2007, Marshall and Randhir 2008, Chu et al. 2010, Du et al. 2012), the uncertainties associated with the land use change models can affect the hydrologic simulation results (De Rosa et al. 2016). The availability of numerous Landsat images over a long term, along with the advancement of classification algorithms, increases the possibility to create more accurate continuous land cover maps (Phiri and Morgenroth 2017). Compared with model-based approaches, supervised classifiers are more widely used due to the robustness and accuracy of its classifications (Weinmann et al. 2015).

Therefore, the objective of this study is to systematically evaluate the impacts of urbanization and climate change on streamflow by leveraging the advantages of both paired catchments analysis and physically based distributed hydrological modeling. Two representative neighboring river basins in Texas—one undergoing fast urbanization, while the land cover of the other basin has barely changed—were selected for the paired catchment analysis. The DHSVM model, which has an explicit urban module component, was adopted for generating simulation results. To best represent the urbanization processes, annual land cover maps were constructed from Landsat image classifications continuously from 1984 to 2011. Specifically, the study focuses on answering the following questions:

1) What are the joint impacts of urbanization and climate change on streamflow?

2) How does climate change alone affect streamflow?

3) What is the impact of urbanization on streamflow?

4) What is the elasticity of streamflow to precipitation in the study region and how does the urbanization influence the elasticity?

## 2. STUDY AREA

Texas is the largest state (676,587 $km^2$) in the Contiguous United States (CONUS) and its precipitation is characterized by drastic spatial and temporal variations. The average annual precipitation increases from 254 mm in West Texas to 1524 mm in East Texas (1981 – 2010; TWDB 2018). Most of the Texas population resides in east Texas — in which extreme events have led to numerous catastrophic floods in the past century. A recent event was the devastating Hurricane Harvey (August 25 to 31, 2017), which resulted in damages of around 125 billion dollars and was ranked as the second costliest tropical cyclone in the U.S history (1900 – 2017) (Eric et al. 2017).

The San Antonio River Basin (SARB) and the Guadalupe River Basin (GRB) (Figure 1) are two adjacent river basins which are located near the Balcones Escarpment in south-central Texas (the SARB: 28.50-29.96°N, 96.89-99.61°W; the GRB: 28.53-30.26°N, 96.86-99.69°W). The San Antonio River merges into the Guadalupe River about 10 miles upstream from San Antonio Bay (located on the perimeter of the Gulf of Mexico). Both basins have the same humid and subtropical climate (Table 1) and similar precipitation climatology (Figure 2). From 1966 to 2011, the average daily temperature was 21$^oC$ in both basins, while the average daily relative humidity in the GRB (65%) was only 3% higher than that in the SARB (Livneh et al. 2013). In both basins, the dominant vegetation types are grass and shrub, and the main soil type is clay which has low hydraulic conductivity and can easily lead to flood (soil texture of the study area is shown in Appendix A). Because the study area is close to the Gulf Coast, it is subject to tropical storms and hurricanes (especially in the fall season) (Guannel et al. 2014). During October 17$^{th}$ -18$^{th}$, 1998, a catastrophic flood struck the study area. The strong storm was

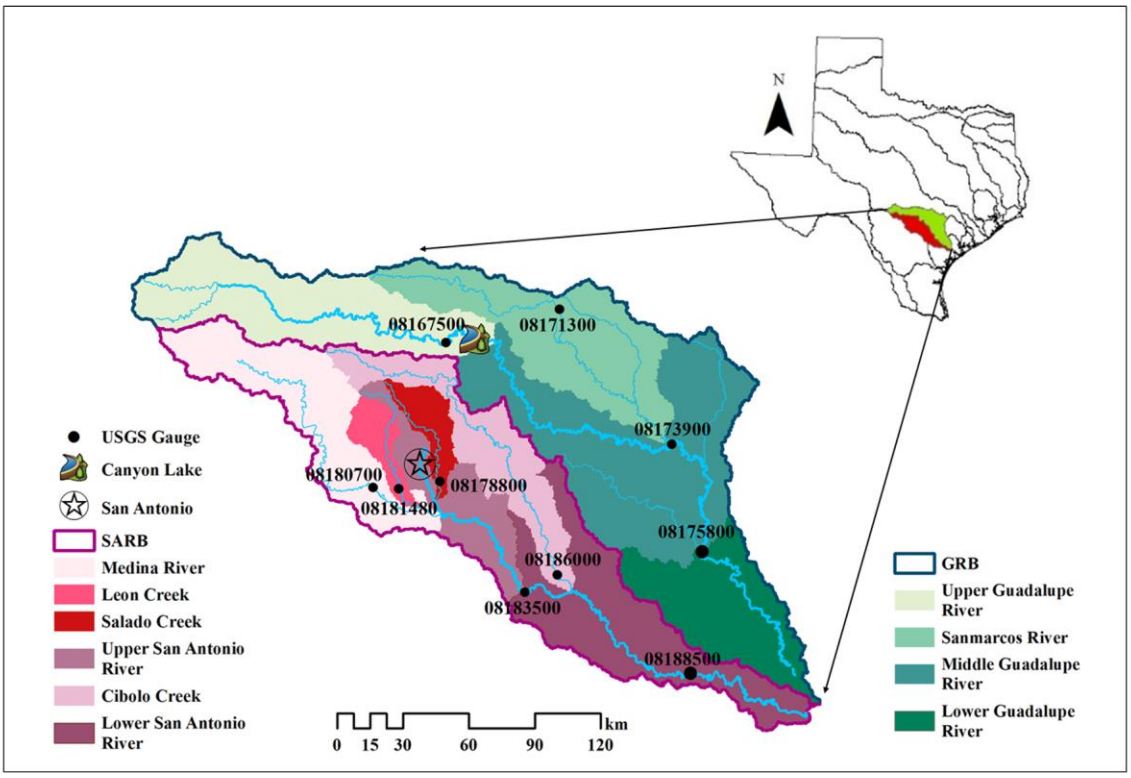


Figure 1 Map of the study area, which includes the San Antonio River Basin (SARB) and the Guadalupe River Basin (GRB).

| River Basin | Precipitation | | Temperature ($^{o}$C) | | | | |
|---|---|---|---|---|---|---|---|
| | Annual Mean (mm/year) | Wettest Month(s) | Annual Mean | Daily Mean (min) | | Daily Mean (max) | |
| | | | | January | July | January | July |
| SARB | 762 | May, Sep | 21 | 5 | 23 | 18 | 36 |
| GRB | 813 | May, Sep | 26 | 3 | 22 | 16 | 35 |

Table 1 Climatic conditions in the SARB and the GRB (TWDB 2018).

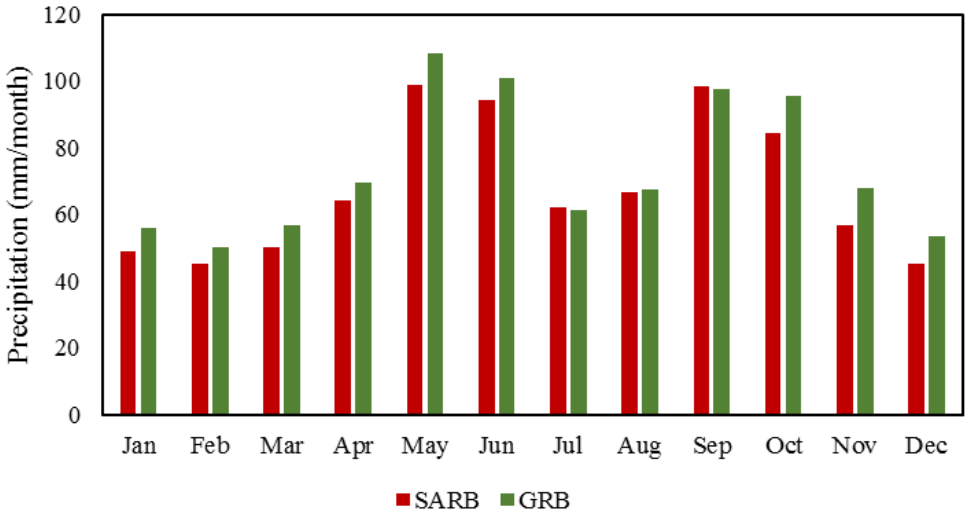

Figure 2 Monthly precipitation climatology in the GRB and the SARB (1966 – 2011). Data are adopted from Livneh et al. 2013.

triggered by two hurricanes — Hurricane Madeline (in the Eastern Pacific near the tip of Baja California) and Hurricane Lester (in the Eastern Pacific near Acapulco, Mexico). The peak streamflow in October 1998 equals or exceeds the 100-year recurrence period for total 13 stations in the study area (USGS 2014).

The SARB has a drainage area of 10,826 $km^2$. The elevation of the basin ranges from 4 m to 693 m above sea level (Zhao et al. 2016), and the average rainfall is around 815 mm/year (1966 to 2011) (Livneh et al. 2013). There are six sub-basins (i.e., the Medina River Basin, the Leon Creek Basin, the Salado Creek Basin, the Upper San Antonio River Basin, the Cibolo Creek Basin and the Lower San Antonio River Basin) in the SARB (Figure 1). The city of San Antonio, which is the second most populous city in Texas, lies in the center of the region containing the Leon Creek Basin, Salado Creek Basin, and Upper San Antonio River Basins. The city of San Antonio has experienced rapid urbanization over the past several decades, with the urban population doubling from 0.65 million to 1.3 million people (1970 to 2010; Thomas et al. 2013). Meanwhile, based

on the comparison of land cover maps, the urban area has almost tripled in size during this period (Price et al. 2007, Jin et al. 2013). Specifically, from 2000 to 2010, among the ten largest cities in the U.S, San Antonio had the fastest population growth (+15.9%) with an increase of 181,893 people (Castro et al. 2012).

The GRB has a drainage area of 15,418 $km^2$. The elevation of the basin ranges from 1m to 735 m above sea level, and the average rainfall from 1966 to 2011 is around 884 mm/year (Livneh et al. 2013). The GRB consists of four sub-basins: the Upper Guadalupe River basin, the San Marcos River basin, the Middle Guadalupe River Basin and the Lower Guadalupe River Basin (Figure 1). Although the SARB and the GRB share similar climate patterns and geology, there is no large city in the GRB. In contrast to the SARB, the population of the GRB was approximately 240 thousand people in 1970 and only increased to 330 thousand people by 2010 (Thomas et al. 2013). During the same period, the impervious area of the GRB increased slightly from 55 $km^2$ to 81 $km^2$. In addition, there is a flood reservoir – Canyon Reservoir **(**29.86°N, 98.20°W) – located in the Upper Guadalupe River. This reservoir is owned by the United States government and is operated by the U.S. Army Corps of Engineers. The main purpose of this reservoir is flood control. The reservoir has a total storage capacity of 467,306,365 $m^3$, encompassing a surface area of 33.62 $km^2$ at the conservation pool elevation (84.45 m above mean sea level) (TWDB 2018).

# 3. METHODS AND DATA

This chapter introduces the hydrological model, model input data, the change point method, and the study design.

## 3.1 Hydrological Model

In this study, the high-resolution Distributed Hydrology Soil Vegetation Model which is embedded with a multi-purpose reservoir module (DHSVM-Res; Wigmosta et al. 1994; Zhao et al. 2016) was used to simulate the streamflow under the changing environment (i.e., urbanization and climate change). DHSVM-Res is an open-source, physically based distributed model which simulates full energy and water balance cycles over a basin/sub-basin scale. The latest version of DHSVM-Res takes into account of the snow accumulation/melt, the land use land cover (LULC), stream temperature, and reservoir flow regulation (Cao et al. 2016; Frans et al. 2016; Zhao et al. 2016).

There are two advantages of DHSVM-Res for supporting this study: the urban module (Cuo et al. 2008) and the reservoir module (Zhao et al. 2016). In Cuo et al. (2008), a land cover type “urban” (i.e., including dense/medium/light urban) was added to address hydrological processes associated with the impervious area. For each “urban” pixel, the fraction of impervious area and the fraction of water stored in flood detention are specified. The fraction of impervious area determines the amount of surface runoff, which is diverted to detention storage and follows the designed detention process. Then, based on the outflow from the detention, the runoff to the nearest channel can be calculated. In Zhao et al. (2016), a multi-purpose (e.g., flood control, water supply) reservoir module was integrated into DHSVM. The reservoir module consists of three components: the evaporation scheme, the release scheme, and the storage calculation

(calculating the overall mass balance of the reservoir storage). The above advantages make DHSVM-Res an ideal tool to simulate both streamflow and water resources (e.g., reservoir regulations of Canyon Lake) over the study area.

## 3.2 Input Data

DHSVM-Res can be set up at a high spatial resolution (e.g., 10 – 200m) and at a sub-daily time step (e.g., 1 – 24 hour). In this study, the simulations were all set at a 200-meter spatial resolution and at a 3-hourly time step for both the SARB and the GRB. There are three sets of input data: land data, reservoir parameters, and meteorological forcing data.

### *3.2.1 Land Data*

The land data include elevation, vegetation, and soil data. The elevation data – Digital Elevation Model (DEM) map – was adopted from the Shuttle Radar Topography Mission (SRTM) 30-meter resolution product (Jarvis et al. 2008), and then was resampled to 200 meters. The basin mask was created based on the DEM using ArcMap. Then, flow direction, stream network, and soil depth files were generated from the DEM using the python scripts by Duan (2017). The soil texture data was obtained from the Soil Survey Geographic Database (SSURGO) (Nauman et al. 2018). SSURGO was selected because it is the most detailed soil geographic dataset developed by the National Cooperative Soil Survey.

In this study, land cover data were acquired from three sources. The first source is the USGS National Land Cover Database (NLCD), which includes NLCD1992, NLCD2001, NLCD2006, and NLCD2011 (Vogelmann et al. 2001, Homer et al. 2007, Fry et al. 2011, Jin et al. 2013). The NLCD products were generated from Landsat

images by the Multi-Resolution Land Characteristics Consortium (MRLC). The second source is the USGS Enhanced Historical Land-Use and Land-Cover Datasets, which depict land use and land cover from the 1970s to 1980s (referred to as LC1970s hereinafter). The LC1970s was derived from NASA high-altitude aerial photographs and National High-Altitude Photography (NHAP) program photographs (Price et al. 2007). The third data source is the Continuous Land Cover Series (CLCS), which were constructed in this study using Landsat 5 Thematic Mapper imagery for the San Antonio City Area from 1984 to 2011.

The CLCS maps were generated by overlaying the 30-m Landsat classification based urban land cover (ULC) on LC1970s (the baseline map). In this way, all non-urban pixels of CLCS remain the same as that of LC1970s. The detailed algorithm is summarized in the following five steps (Figure 3).

1) Creating annual composite image.

For each year from 1984 to 2011, a composite image was constructed using the Landsat surface reflectance images. The temporal resolution of the Landsat product is 16-day, thus there are around 20 Landsat images for each year. In this study, seven images with the least amount of cloud cover fraction were selected. Second, for each of the seven images, the contaminated pixels (i.e., cloud, cloud shadow, and snow) were removed using the Fmask algorithm (Zhu et al. 2014) – an algorithm for identifying cloud, cloud shadow, water, and snow pixels from Landsat images. Afterward, the composite image was formed by calculating the median value for each pixel from the seven images.

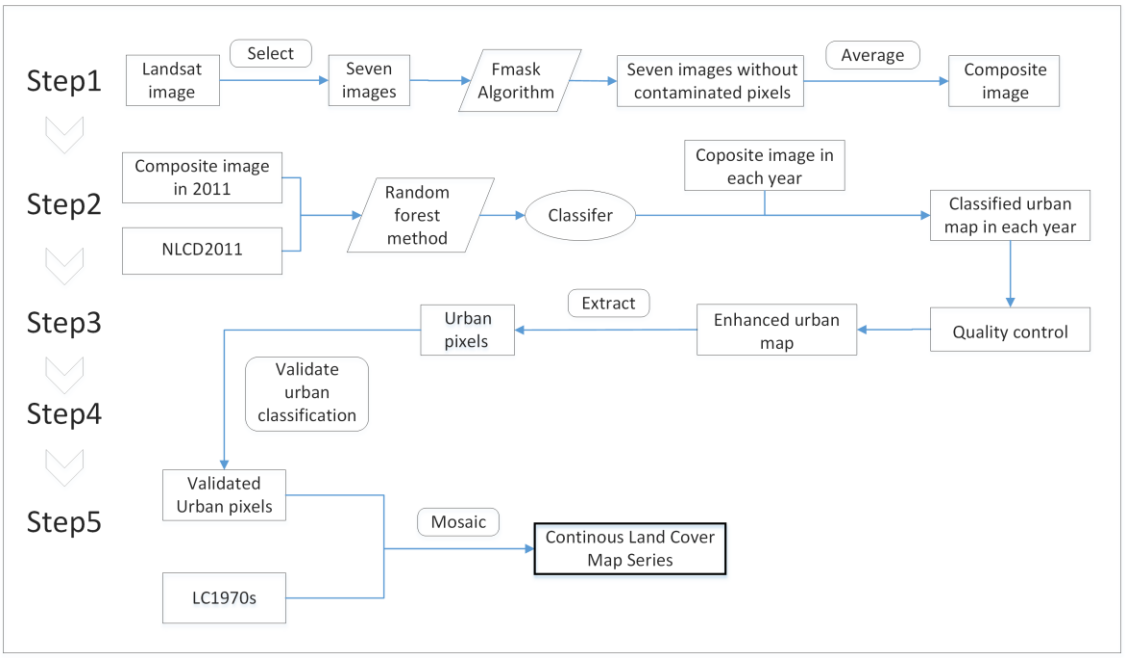


Figure 3 Flowchart of the main steps for generating CLCS. Step 1: Creating annual composite image; Step 2: Classifying urban pixels; Step 3: Post-processing to enhance urban classifications; Step 4: Validating urban classification; and Step 5: Constructing CLCS.

2) Classifying urban pixels.

In this step, the Random Forest (RF) supervised classification method was utilized to classify the urban pixels. RF classification method has been widely used in the recent two decades due to its robustness and successful application to land cover classification (Du et al. 2015; Pal 2005; Breiman 2001). Basically, the "Forest" represents an ensemble of Decision Trees and the "Forest" is trained by the RF classifier with the "bagging" method (i.e., a combination of different learning models). Randomness is incorporated to the method by randomly selecting a subset of training data (Donges 2018). One key advantage of RF is that it can avoid overfitting by creating subsets of the features and growing smaller trees using these subsets.

In the NLCD, class 21 (developed, open Space), class 22 (developed, low intensity), class 23 (developed, medium intensity), and class 24 (developed, high

intensity) are used to represent urban land covers with different impervious area (Fry et al. 2011). To simplify the following steps, all of the other non-urban land cover classes in NLCD were assigned as class 0. For each of the four urban classes, 500 pixels within the San Antonio City Area were randomly selected from the NLCD2011 as training data. Six Landsat TM bands were selected, which include three visible bands (bands 1, 2, 3), one near-infrared band (band 4), and two shortwave infrared bands (bands 5 and 7). These NLCD2011 training data were paired with the corresponding pixels from the 2011 composite image to generate random forest classifier, which was used to classify urban pixels in other composite images.

3) Post-processing to enhance urban classifications.

To enhance the accuracy of the classified urban pixels, post-processing (quality control) is necessary to eliminate the misclassified pixels. Two rules were followed in this process: (1) the urban land cover pixels are not likely to change back to non-urban types; and (2) the developed urban areas are not likely to change back to less developed types. Because it is difficult to control the quality of the map at the beginning of the study period, the first two years (1984 and 1985) were considered as the “spin up” period (Figure 4). Through this enhancement, the consistency among urban pixels from different years is maintained.

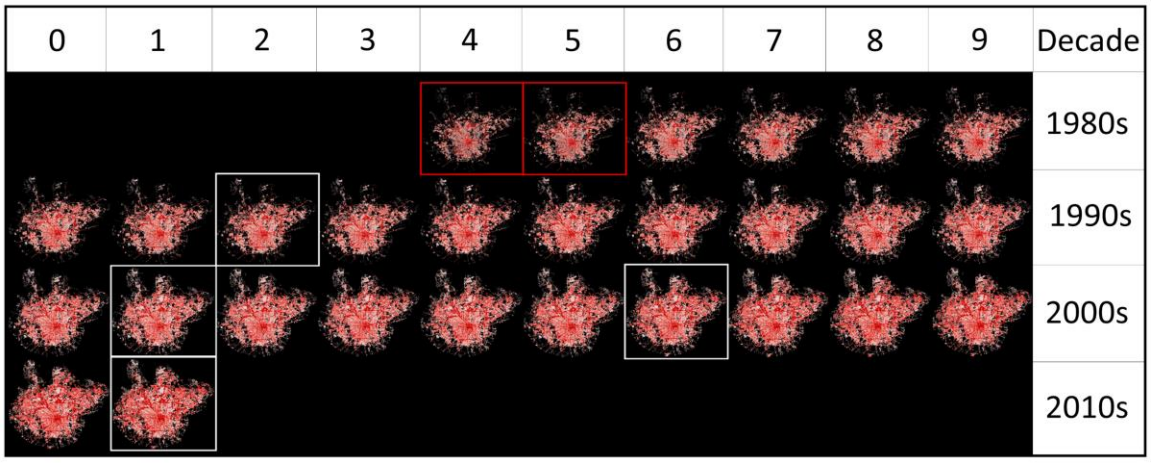


Figure 4 The annual ULC maps generated from Landsat classifications from 1984 to 2011. Numbers "0-9" represent the order of the year in each decade; the maps outlined in red represent the "spin up" year; the maps outlined in white represent NLCD land cover maps.

4) Validating urban classification.

The validation was conducted by comparing the classification of each pixel from ULC2001 and ULC2006 with the corresponding pixels from NLCD2001 and NLCD2006 respectively.

As shown in Table 2, the ULC2001 has a success rate ranging from 82.61% to 96.09%, with the skill increasing as the urban class becomes denser. The success rate of the ULC2006 ranges from 89.26% to 93.90%. For ULC2001, most of the errors of each urban class are associated with assigning a nearest less dense urban class, which suggests an underestimation of the impervious area. According to Table 3, the errors of the dense urban pixels (classes 23 and 24) in ULC2006 are similar to those in ULC2001 (i.e., underestimation). However, most errors of the light urban pixels (classes 21, 22) in ULC2006 are from the nearest denser urban class, which is different from ULC2001.

Overall, in the constructed ULC2001, 94.49% of the pixels from classes 23 – 24 have the same class value of NLCD2001, with only 86.46% pixels from class 21 – 22

matching the NLCD2001. In the case of ULC2006, the percentages are 92.61% and 90.38%, respectively. Hence, this indicates that the classification method has better results in the urban pixels with denser urban class. The main reason for this is that it becomes more challenging to classify urban pixels with a large fraction of other land cover types (e.g., grass, tree, rock).

5) Constructing CLCS.

In this last step, the urban pixels from the ULC maps were superimposed on the LC1970s using ArcGIS. This way, the CLCS were constructed successfully and can be employed for parameterizing DHSVM-Res.

| Pixel comparisons between constructed ULC2001 and NLCD2001 | | Constrcuted ULC2001 | | | | | | | | | | Total pixels of NLCD 2001 |
|---|---|---|---|---|---|---|---|---|---|---|---|---|
| | | 0 (non-urban pixels) | | 21 (Developed, Open Space) | | 22 (Developed, Low Intensity) | | 23 (Developed, Medium Intensity ) | | 24 (Developed,High Intensity) | | |
| | | Pixel numbers | Match rate (%) | Pixel numbers | Match rate (%) | Pixel numbers | Match rate (%) | Pixel numbers | Match rate (%) | Pixel numbers | Match rate (%) | |
| NLCD2001 | 0 | **1171925** | **97.45%** | 23836 | 1.98% | 4951 | 0.41% | 1596 | 0.13% | 312 | 0.03% | 1202620 |
| | 21 | 72095 | 13.53% | **440145** | **82.61%** | 9244 | 1.73% | 10371 | 1.95% | 951 | 0.18% | 532806 |
| | 22 | 9424 | 2.34% | 13789 | 3.42% | **368925** | **91.56%** | 7081 | 1.76% | 3696 | 0.92% | 402915 |
| | 23 | 2679 | 1.07% | 3012 | 1.21% | 9595 | 3.85% | **233406** | **93.62%** | 625 | 0.25% | 249317 |
| | 24 | 689 | 0.51% | 552 | 0.41% | 785 | 0.58% | 3287 | 2.42% | **130656** | **96.09%** | 135969 |
| Total pixels of constrcuted ULC2001 | | 1256812 | | 481334 | | 393500 | | 255741 | | 136240 | | |

Table 2 Validation of the ULC2001.

| Pixel comparisons between constructed ULC2006 and NLCD2006 | | Constrcuted ULC2006 | | | | | | | | | | Total pixels of NLCD 2006 |
|---|---|---|---|---|---|---|---|---|---|---|---|---|
| | | 0 (non-urban pixels) | | 21 (Developed, Open Space) | | 22 (Developed, Low Intensity) | | 23 (Developed, Medium Intensity ) | | 24 (Developed,High Intensity) | | |
| | | Pixel numbers | Match rate (%) | Pixel numbers | Match rate (%) | Pixel numbers | Match rate (%) | Pixel numbers | Match rate (%) | Pixel numbers | Match rate (%) | |
| NLCD 2006 | 0 | **1060892** | **96.27%** | 23479 | 1.95% | 10558 | 0.88% | 5550 | 0.46% | 1503 | 0.12% | 1101982 |
| | 21 | 12795 | 2.40% | **468136** | **89.26%** | 34620 | 6.50% | 7867 | 1.48% | 1046 | 0.20% | 524464 |
| | 22 | 5909 | 1.47% | 7493 | 1.86% | **391805** | **91.49%** | 21415 | 5.32% | 1632 | 0.41% | 428254 |
| | 23 | 1544 | 0.62% | 6516 | 2.61% | 12921 | 5.18% | **283625** | **91.31%** | 6016 | 2.41% | 310622 |
| | 24 | 312 | 0.23% | 620 | 0.46% | 1762 | 1.30% | 6959 | 5.12% | **148652** | **93.90%** | 158305 |
| Total pixels of constrcuted ULC2006 | | 1081452 | | 506244 | | 451666 | | 325416 | | 158849 | | |

Table 3 Validation of the ULC2006.

### *3.2.2 Reservoir Parameters*

The reservoir configuration was set up for Canyon Lake, the main reservoir in the GRB (Figure 1). The reservoir storage, elevation, and surface area data were acquired from the Texas Water Development Board (TWDB) and were used to derive the reservoir rating curve for Canyon Lake. The fitted storage – area and storage – elevation curves are shown in Appendix B. The pertinent data were obtained from the United States Army Corps of Engineers (USACE). The storage capacity of Canyon Lake ($1.50 \times 10^9$ $m^3$) is divided into the surcharge pool ($1.1 \times 10^8$ $m^3$), the flood control pool ($9.1 \times 10^8$ $m^3$), the conservation pool ($4.8 \times 10^8$ $m^3$), and the inactive pool ($8.7 \times 10^5$ $m^3$). In addition, four downstream control points (i.e., New Braunfels NBRT2, Gonzales GNLT2, Cuero CUET2, and Victoria VICT2; National Weather Service 2018) with the same channel streamflow capacity (340 $m^3/s$; USACE 2017) were designated to represent the downstream flow-control operations. With regard to sedimentation, the survey suggests that the conservation volume of Canyon Lake has decreased by 1.9% since 1964 and the sedimentation rate was about $1.89 \times 10^5$ $m^3$/year (TWDB 2001).

### *3.2.3 Forcing Data*

Two types of forcing data – observation-based and synthetically generated – were adopted to drive the hydrological model. Observation-based forcing data were used for model calibration and validation, as well as serving as the "benchmark". Synthetic forcing data were used to eliminate the climatic inter-annual variability, such that the DHSVM results can be analyzed for the impact of urbanization alone. Both datasets contain a full set of meteorological fields (i.e., air temperature, wind speed, relative humidity, incoming shortwave radiation, incoming longwave radiation, soil temperature,

and precipitation). The only difference between these two types of forcing datasets is the precipitation. These two datasets were both disaggregated to 3-hourly time step and 200m resolution.

The observation-based forcing data are available over the contiguous United States (CONUS) at 1/16° spatial resolution with a daily time step from 1915 to 2011 (Livneh et al. 2013). After the disaggregation, the data were used to drive DHSVM-Res during the calibration/validation processes. Besides, these forcing datasets were also used in the simulation under fixed LC1970s, which served as the "benchmark" for extracting the impact of climate change on streamflow.

The synthetic forcing data are the same as the observation-based forcing data except that precipitation was replaced by the rescaled precipitation. The purpose of generating synthetic forcing data is to eliminate the impact from the climatic inter-annual variability. Three representative years – dry, normal, and wet – were selected from the observation-based forcing data. To rescale the precipitation time series based on the above representative years, the cumulative distribution function (CDF) mapping technique (Rossum 1995) was utilized (Figure 5d).

Specifically, three steps were carried out to derive a series of synthetic forcing data:

1) Selecting representative precipitation years.

Three representative precipitation years (Table 4) were selected based on the long-term precipitation climatology. For example, the year 1978 was selected to represent the normal year because its annual precipitation is close to the multi-year average precipitation (815 mm; 1966 - 2011).

2) Rescaling precipitation via CDF mapping.

For each of the above representative years, the CDFs of the daily precipitation were calculated after Rossum (1995) (Figure 5a - c). These three CDFs were then used as references for generating new daily precipitation time series from the observed data (1984-2011). Figure 5d shows an example in which the observed precipitation data in a randomly selected year (1968) at a random location (29.84375º N, 99.40625º W) was rescaled to match the CDF in 1978 (normal year). By applying this CDF mapping for each pixel within the basin for each year during the period of 1984-2011, a synthetic forcing dataset characterized with a normal year precipitation was generated. This procedure was repeated for each of the three representative years. Thus, each of the time series has a fixed annual precipitation which matches that from the corresponding representative year. It means that there is no inter-annual variation in terms of precipitation amount, even though the precipitation occurrence (frequency) follows a similar pattern as the historical observations.

3) Perturbing the synthetic forcing time series.

Each of the three rescaled precipitation time series was further perturbed by +/- 10%, +/-20%, and +/-30%, respectively. In this way, there were twenty-one rescaled precipitation time series in total (seven precipitation time series for each representative climate). They were then combined with the other six fields (i.e., air temperature, wind speed, relative humidity, incoming shortwave radiation, incoming longwave radiation, and soil temperature) from the corresponding observation-based forcing data to generate full synthetic forcing data for DHSVM-Res simulations.

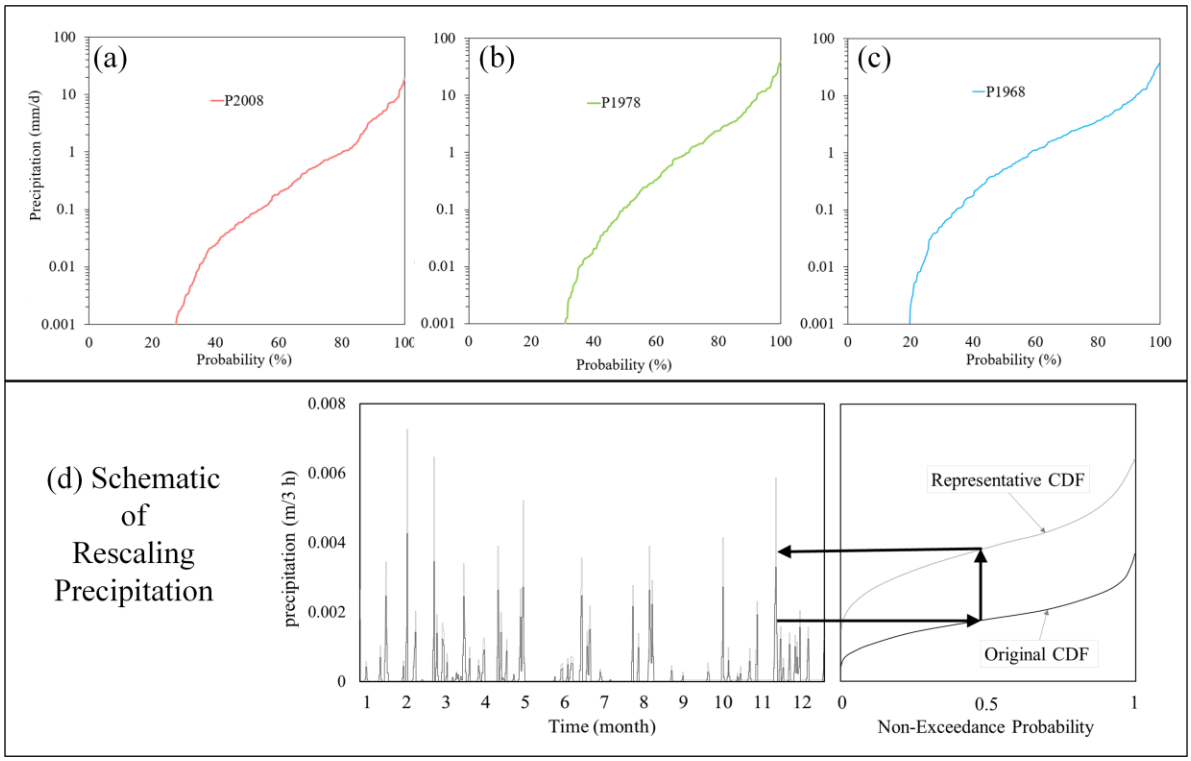


Figure 5 (a) Precipitation for 2008 (b) Precipitation for 1978 (c) Precipitation for 1968 (d) Schematic of CDF mapping technique for mapping year 1968 to representative year 1978 at 29.84375º N, 99.40625º W.

| Genre | Year | Annual Precipitation (mm/year) |
|---|---|---|
| Normal Year | 1978 | 815 |
| Wet Year | 1968 | 1025 |
| Dry Year | 2008 | 398 |

Table 4 Table of representative precipitation years.

## 3.3 Change Point Detection Method

The change point (CP) detection method (R package; Killick and Eckley 2014) is used to detect abrupt changes in precipitation and streamflow time series. Specifically, three sets of variables were analyzed using this method. First, the CP of the observed precipitation in each basin was identified to determine if the two basins have undergone the same climatic change. Second, the observed Monthly Maximum Streamflow (MMS-Obs) of the GRB and the SARB were examined to evaluate the combined effect of

climate change and urbanization on streamflow. Third, the simulated Monthly Maximum Streamflow (MMS-LC1970) with a fixed land cover map, which is under the assumption of no urbanization in both basins were analyzed to help separate the climatic effect and urbanization effect on streamflow.

In this study, the single CP of mean value along the time series data was adopted because it is easier to compare the CP results of streamflow from different scenarios. According to Killick and Eckley (2014), the process of the single CP detection can be considered as a hypothesis test. The null hypothesis, H0, represents that there is no CP and the alternative hypothesis, H1, represents that there is a single CP. If there is a time series, $x_{1:n} = (x_1, x_2, \dots, x_n)$, a CP can be found in this sequence of data at any time point, $\tau \in \{1, 2, \dots, n-1\}$. In the case of the null hypothesis (H0), the maximum log-likelihood can be defined as $(x_{1:n}|\hat{\theta})$ , where $p(\cdot)$ is the probability density function which is related to the distribution of the data and $\hat{\theta}$ is the maximum likelihood estimate of the parameters. If there is a CP at $\tau_1$, with $\tau_1 \in \{1, 2, \dots, n-1\}$, the function of the maximum log-likelihood for the given $\tau_1$ can be defined as:

$$ML(\tau 1) = logp(x_{1:\tau 1}|\hat{\theta}_1) + logp\left(x_{(\tau 1+1):n}\middle|\hat{\theta}_2\right) \quad (1)$$

Because the location of CP is discrete in the time series, the value of $ML(\tau 1)$ under the alternative hypothesis (H1) can be estimated by calculating $max_{\tau 1}\, ML(\tau 1)$. According to Killick and Eckley (2014), the test statistic for maximum likelihood estimation λ is defined as

$$\lambda = 2\left[\, max_{\tau 1} ML(\tau 1) - \, logp(x_{1:n}|\hat{\theta})\right] \quad (2)$$

Then, a threshold $c$ is chosen by designing the penalty values (Birge and Massart 2007). The null hypothesis is rejected if $\lambda > c$ at a certain significance level, which indicates

that a single CP is detected. The position of the CP is considered as $\hat{\tau}_1$ which maximizes $ML\ (\tau 1)$. However, the proper value for this parameter *c* is still an open research question (Killick and Eckley 2014).

## 3.4 Study Design

The DHSVM-Res was first calibrated and validated. Then, DHSVM-Res simulations were conducted under the designed scenarios. Later, the change point analysis method was applied to the simulated/observed streamflow and the observed precipitation. In the end, the elasticity test of streamflow to precipitation was conducted based on the results of the simulations.

### *3.4.1 Calibration and Validation*

In this part, calibration and validation were conducted only for the GRB, as the calibrated parameters for the SARB were adopted from Zhao et al. (2016). For this process, three typical error statistics were used for evaluating the performance of the DHSVM parameters: the relative bias (RB), the coefficient of determination ($R^2$), and the Nash–Sutcliffe efficiency (NSE) (Nash and Sutcliffe 1970). Both the simulated streamflow and reservoir storage were compared with the observed data. Considering that MMS is mainly focused on in this study, the $R^2$ and NSE were considered first, because they are very sensitive to peak flows (Krause et al. 2005). When the $R^2$ and NSE were maximized, the absolute value of RB was minimized and it was required to be less than 25%. RB was not considered in the first place because this statistic is used to evaluate the total amount of streamflow, and there is a limitation in this hydrological model that the base flow cannot be simulated well. Also, the value of $R^2$ was similar to the value of NSE

during the calibration process for streamflow in many cases, so they were considered jointly (Krause et al. 2005). Specifically, these objective functions are defined as follows:

$$RB = \frac{\sum_{t=1}^{T}(Q_m^t - Q_o^t)}{\sum_{t=1}^{T} Q_o^t} \quad (3)$$

$$R^2 = \left(\frac{\sum_{t=1}^{T}(Q_o^t - \overline{Q_o})(Q_m^t - \overline{Q_m})}{\sqrt{\sum_{t=1}^{T}(Q_o^t - \overline{Q_o})^2 \sum_{t=1}^{T}(Q_o^t - \overline{Q_o})^2}}\right)^2 \quad (4)$$

$$NSE = 1 - \frac{\sum_{t=1}^{T}(Q_0^t - Q_m^t)^2}{\sum_{t=1}^{T}(Q_o^t - \overline{Q_o})^2} \quad (5)$$

Where, $Q_o$ is the observed streamflow, $Q_m$ is the modeled streamflow, $\overline{Q_o}$ is the mean of the observed streamflow time series, $\overline{Q_m}$ is the mean of the simulated streamflow time series, and $t$ is the order of the time series. In addition to the efficiency criteria, the calibration process also relied on the subjective criteria (i.e., the observed and the simulated values were plotted and visually evaluated).

Three kinds of parameters need to be calibrated: soil parameters, vegetation parameters, and reservoir parameters. The primary soil parameters include maximum infiltration, porosity, and hydraulic conductivity. The main vegetation parameters are the maximum/minimum stomatal resistance, the leaf area index, and the canopy attenuation. The reservoir parameters are the discharge rate and the flood inflow threshold. Because some of the water demand data (including industrial, agricultural, municipal and hydropower water use) are unavailable, the water demand data was first calibrated at a monthly level and then divided to a daily.

The parameters were all calibrated during the period from January 1st 2001 to December 31th 2011. The calibration of soil/vegetation parameters was conducted at a sub-basin scale because the primary soil/vegetation types are different in each sub-basin. After the soil/vegetation parameters were calibrated, the reservoir parameters were

calibrated by comparing the simulated monthly volume and the observed data. Specifically, because there is no available inflow data for Canyon Lake, the simulated streamflow at the location of the reservoir was generated using the calibrated soil/vegetation parameters. The validation of DHSVM-Res focuses on one downstream station (USGS 08175800) which has a sufficiently long record. Finally, validation was conducted from January 1$^{st}$ 1966 to December 31$^{th}$ 2011.

The DHSVM-Res inputs for model calibration and validation are summarized in Table 5. The results of calibration and validation over the GRB are shown in section 4, while the calibrated parameters for the SARB were adopted from Zhao et al. (2016).

| Process/Scenario | Basin | Land cover map | Forcing source | Periods |
|---|---|---|---|---|
| Calibration | GRB | NLCD2006 | Livneh et.al (2013) | 2001-2011 |
| Validation | GRB | LC1970s | Livneh et.al (2013) | 1966-1985 |
| | | NLCD1992 | | 1986-1996 |
| | | NLCD2001 | | 1997-2003 |
| | | NLCD2006 | | 2004-2007 |
| | | NLCD2011 | | 2008-2011 |

Table 5 Summary of the DHSVM-Res inputs for calibration and validation.

### *3.4.2 DHSVM Simulations under Designed Scenarios*

The calibrated parameters were used for simulations under three sets of scenarios. In the first set, simulations were carried out under a fixed land cover map (i.e., LC1970s) from 1966 to 2011 for both basins. In the second set, a series of simulations with the same continuous CLCS but under different synthetic forcings was conducted from 1985 to 2011 for the SARB. The only difference between the third and the second set is that in

the third set, the continuous annual land cover maps are replaced with the fixed land cover maps (i.e., 1986, 2000, 2011). Although all three sets focus on separating the impacts of climate and urbanization on streamflow, the first set of results were used for the CP analysis, the results from the second and the third set were employed for calculating the precipitation elasticity of streamflow.

1) Change Point (CP) Analysis

First, the CPs of long-term precipitation in both basins were compared. To make the CPs results of precipitation comparable with those from MMS, the precipitation CPs analysis adopted a time of the concentration ($T_c$) concept. The average Tc of a rainfall event in the study area was found to be 24 days (Appendix C). Furthermore, because the CP analysis of this study targets on analyzing the long-term impact but not the historical extreme event, the analysis period was set from 1968 to 2006, with a catastrophic flood event in October 1998 excluded. Meanwhile, the extreme dry period from 2007 to 2011 and two wet years before 1968 were not considered in the analysis period.

Second, for each basin, the CPs of the observation-based and simulated streamflow under fixed LC1970s in the historical period (i.e., the period is the same as the observation-based precipitation) were compared. The observed streamflow reflects the combined impacts of climate change and urbanization on the hydrological process, while the simulated streamflow represents the impact solely from the climate. In this analysis, MMS, which contain the largest streamflow for each month over multiple years, is selected as the indicator of long-time streamflow pattern.

In addition, the annual CP of the impervious area was calculated for the SARB to study the abrupt change of the historical urbanization. This result was further compared

with the CPs of the observation-based streamflow to evaluate the impact from urbanization on streamflow. The annual impervious area is calculated using the generated CLCS based on the four NLCD urban classes. In DHSVM, NLCD class 23 and class 24 are identified as "dense urban", with an impervious area 78%; class 21 and class 22 are classified as "light urban", with an impervious area 27% (Zhao et al. 2016). Thus, the annual impervious area can be calculated after Equation (3):

$$Imperious\ Area = 78\% \times Dense\ Urban\ Area + 27\% \times Light\ Urban\ Area \quad (6)$$

2) Elasticity Test of Streamflow to Precipitation

The elasticity test is only conducted for the SARB in this study. The concept of elasticity was originally introduced by Schaake (1990), which was designed for evaluating the sensitivity of streamflow to changes in climate. The precipitation elasticity of streamflow as:

$$\varepsilon_p(P, Q) = \frac{dQ/Q}{dP/P} \quad (7)$$

Where $Q$ represents the average streamflow and $P$ represents the annual precipitation.

The purpose of the elasticity tests is two-fold: 1) to evaluate the sensitivity of streamflow – when undergoing continuous urbanization – to different precipitation conditions (e.g., dry, normal, and wet) under the same urbanization progress, and 2) to study the effect of the urbanization on the precipitation elasticity. For the first purpose, a series of simulations were conducted under different climate conditions but with the same CLCS from 1984 to 2011. For the second one, a series of simulations were conducted under the fixed urban cover (i.e., ULC1986, ULC2000, ULC2011) with a series of scaled observed precipitation from 1984 to 2011. To make the analysis representative, we focus

on the proportional change of the median value of the simulated MMS time series and the proportional change of the rescaled annual precipitation.

# 4. RESULTS*

## 4.1 Calibration and Validation Results

Hydrographs of the calibration and validation results over the GRB are shown in Figure 6. The error statistics for daily calibration for the Lower GRB suggest that the simulated streamflow are relatively accurate with an $R^2$ of 0.75, an NSE of 0.71, and an RB of 0.05. However, the results for the Blanco River Basin are not as good, with both the $R^2$ and the NSE under 0.60. Meanwhile, it should be noted that the simulated base flows do not agree very well with the observations (Figures 6b and 6c). This can be attributed to the groundwater discharge from Edwards Aquifer that are located close to the USGS Station 08171300. Figure 6e shows the comparison of simulated and observed reservoir storage for Canyon Lake. The good agreement of the simulation and the observation with an $R^2$ of 0.78 indicates that the reservoir parameters in DHSVM-Res are robust.

Overall, the calibration results of the SARB were better than those of the GRB. Specifically, the results from the Lower SARB, which is the most downstream river segment of the SARB, show relatively higher $R^2$ (0.96) and NSE (0.90) values as compared to those of Lower GRB (Table 6). However, the RB of Low SARB was slightly higher than that of the Lower GRB. The primary reason is that the magnitude of groundwater discharge from Edwards Aquifer is lower in the SARB than in the GRB (Maclay and Land 1988).

The validation results (Table 7) indicate that the calibrated parameters are able to simulate the daily streamflow and the peak flows well. The $R^2$ and the NSE of MMS are significantly higher than those of the daily streamflow over both basins.

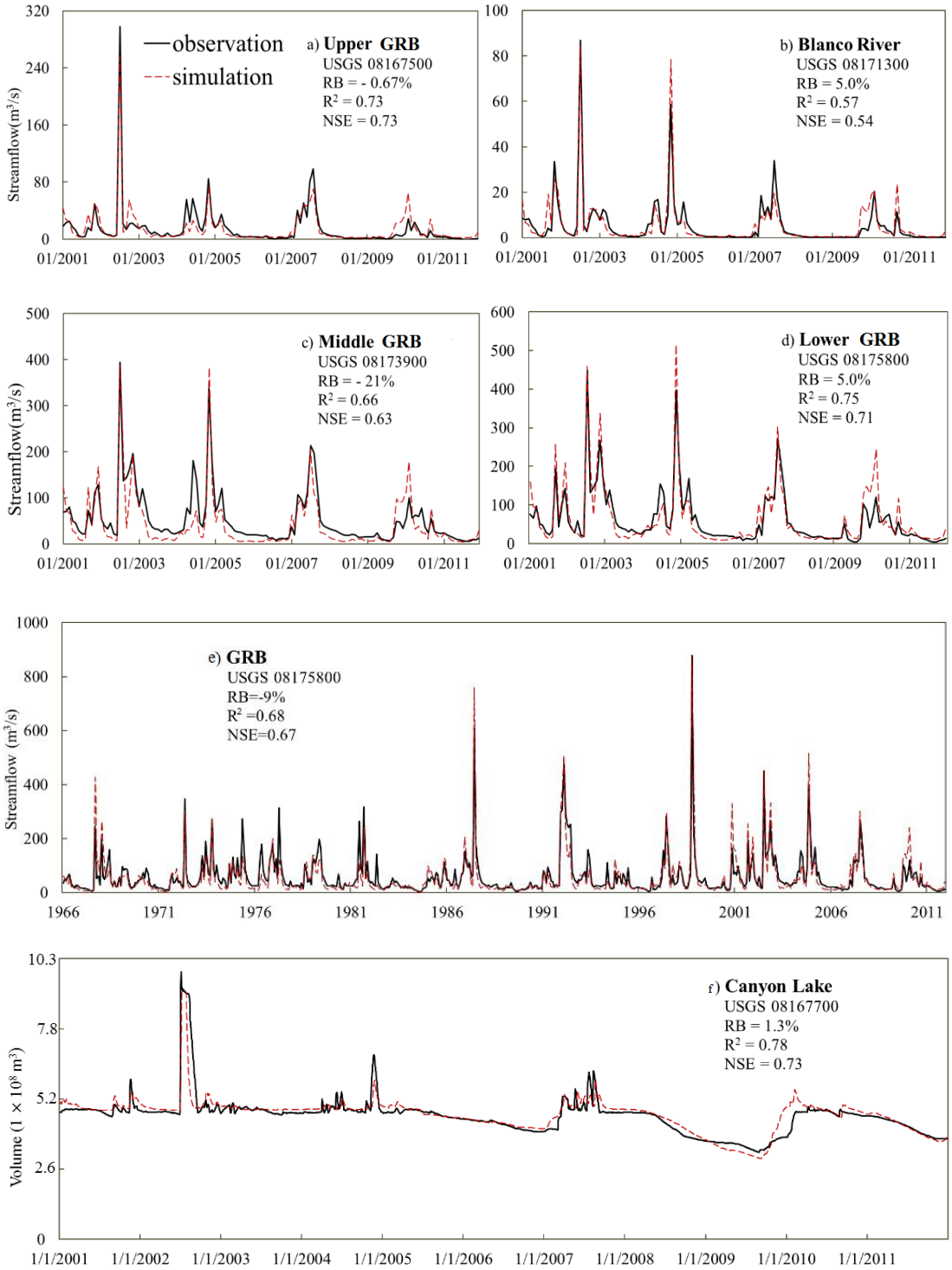


Figure 6 Results of calibration (01/2001-12/2011) and validation (01/1966 - 01/2011) in the GRB. a)– d) Calibration of daily streamflow for each sub-basin. e) Validation of daily streamflow over the entire GRB. f) Calibration of the monthly reservoir volume for the Canyon Lake Reservoir. The statistics in a) – e) are based on daily results but shown in monthly results for better visualization.

| Sub-basins | Medina River | Leon Creek | Salado Creek | Upper SARB | Cibolo Creek | Lower SARB |
|---|---|---|---|---|---|---|
| USGS ID | 08180700 | 08181480 | 08178800 | 08183500 | 08186000 | 08188500 |
| $R^2$ | 0.66 | 0.76 | 0.79 | 0.74 | 0.81 | 0.96 |
| NSE | 0.53 | 0.74 | 0.75 | 0.65 | 0.75 | 0.90 |
| RB | -31% | 22% | 4.0% | 4.0% | 17% | 11% |

Table 6 The calibration results of daily streamflow over the SARB (Zhao et al. 2016).

| Basin / Statistics | Daily runoff | | MMS | |
|---|---|---|---|---|
| | GRB | SARB | GRB | SARB |
| $R^2$ | 0.68 | 0.72 | 0.84 | 0.78 |
| NSE | 0.67 | 0.54 | 0.78 | 0.77 |
| RB | -9% | -14% | -24% | -13% |

Table 7 The validation results over the GRB and the SARB (Zhao et al. 2016).

## 4.2 Results from Change Point Analysis

### *4.2.1 Change Point of the Impervious Area of the City of San Antonio*

With the population growth, the impervious area for the City of San Antonio has been increasing dramatically (Figure 7). The average impervious area was 671 $km^2$ from 1986 to 2011. The CP of the impervious area was detected in 2000 at a significance level of 5%. In the pre-CP period (i.e., 1986-2000), the impervious area had a mean value of 597 $km^2$ while 763 $km^2$ for the post-CP period. The implication of this CP on the streamflow is analyzed in the following section.

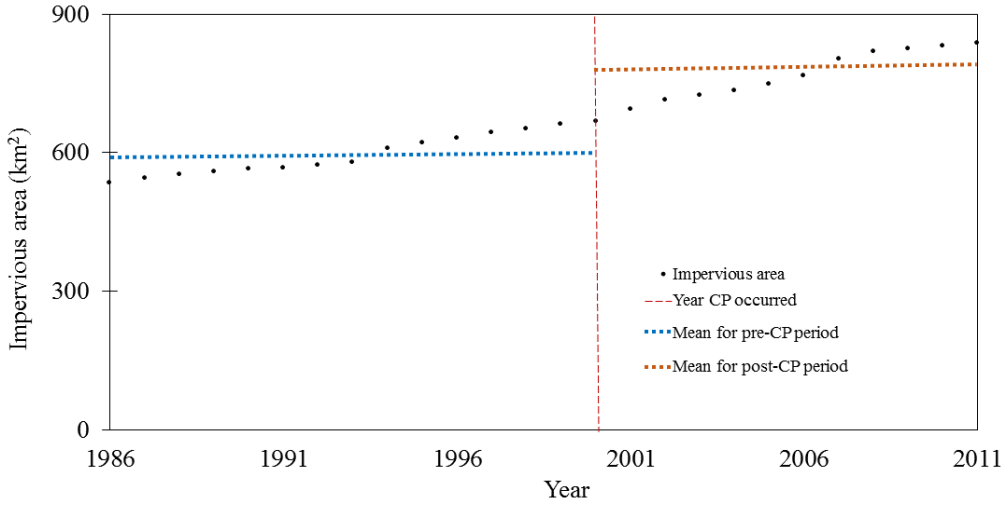


Figure 7 The impervious area of the San Antonio City Area from 1986 to 2011.

### *4.2.2 Change Point of the Hydro-climatic Variables.*

The detected CPs from the time series of precipitation, MMS-LC1970 and MMS-Obs over the GRB and the SARB are shown in Figure 8. The precipitation change points

were first detected for these two neighboring basins to assess the meteorological non-stationarity. In both river basins, March 1991 is the CP for the cumulative 24-day precipitation (at a significance level of 10%), indicating that they share similar precipitation changes during the study period. This suggests that the two basins are suitable for the paired analysis.

With respect to MMS, two sets of change points were calculated (Table 8). It is found that both the MMS-Obs and the MMS-LC1970 of the GRB have the same CPs (i.e., October 1991), which are close to the CP of the precipitation. This is because there are no significant land cover changes in the GRB. Meanwhile, the CP of MMS-LC1970 for the SARB is also October 1991. However, the CP of the MMS-Obs for the SARB is June 2001, which is completely different from the other CPs but similar to the impervious area CP (Section 4.2.1), suggesting remarkable impacts of land cover changes on the peak flow variations.

The timing of these CPs and the mean values of these hydro-climate variables (before and after the CPs) are summarized in Table 8. For the GRB, the mean value of MMS-Obs has increased by 37 $m^3/s$ from the pre-CP period to the post-CP period, which is similar to the difference found from MMS-LC1970 (46 $m^3/s$). In contrast, for the SARB, the difference between the mean value of MMS-Obs over the pre-CP period and the post-CP period (i.e., 56 $m^3/s$) is almost 1.5 times larger than the difference from MMS-LC1970 (i.e., 23 $m^3/s$). These results suggest that urbanization has a significant impact on the change of the MMS over the SARB, especially after 2001.

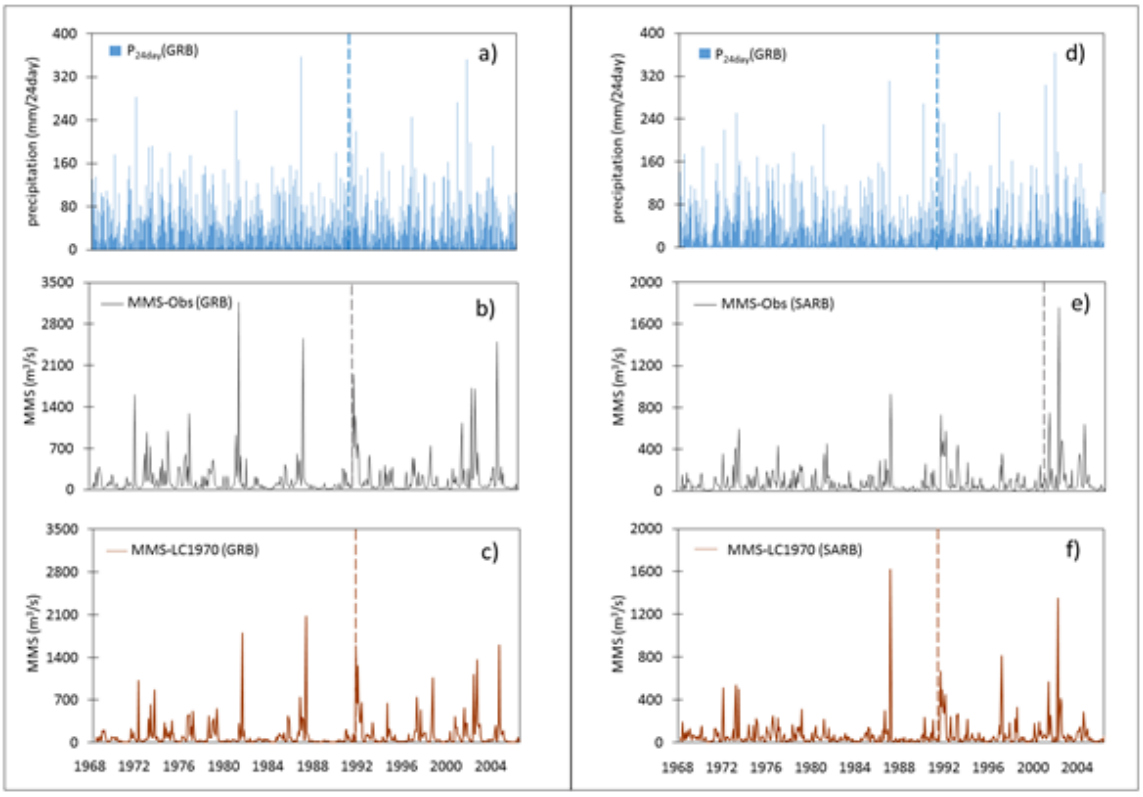


Figure 8 The detected CPs from the precipitation, the MMS-Obs and the MMS-LC1970 over the GRB and the SARB. a) and d): The blue dashed line represents the CPs of the cumulative 24-day precipitation over both basins; b) and e): The brown dashed line represents the CPs of the observed MMS over both basins. c) and f): The grey dashed line represents the CPs of the simulated MMS over both basins.

| Source | Variables | Basin | CP | Mean (Pre-CP) | Mean (Post-CP) |
|---|---|---|---|---|---|
| observed | 24-day precipitation (mm/24day) | GRB | 03/1991 | 57.3 | 59.5 |
| | | SARB | 03/1991 | 52.5 | 54.8 |
| observed | MMS ($m^3/s$) | GRB | 10/1991 | 155 | 192 |
| | | SARB | 06/2001 | 76 | 732 |
| simulated | MMS ($m^3/s$) | GRB | 10/1991 | 100 | 146 |
| | | SARB | 10/1991 | 59 | 82 |

Table 8 Summary of change points (CPs) for the SARB and the GRB.

## 4.3 Results of the Elasticity Test of Streamflow to Precipitation

There are two sets of elasticity tests: one uses synthetic extreme climate conditions (and one normal condition) with the same urbanization progress (i.e., CLCS; Section 3.2.1), for the purpose of assessing the influence of different climate baselines on the elasticity of streamflow to precipitation; the other one utilizes different urban land cover maps (i.e., ULC1986, ULC2000, ULC2011; Section 3.2.1) with the scaled observed precipitations, to evaluate the effect of urbanization on the elasticity.

In the first set, the elasticity of streamflow to precipitation was tested under three types of climatic conditions: dry, normal, and wet (Figure 9). The precipitation data for three representative years (i.e., dry/2008, normal/1978, and wet/1968) were extended to the 27-year study period after the method described in Section 3.2.3. The elasticity values ($\varepsilon_p$) range from 1.5 to 3.0. This indicates that in the long-term hydrological process, when the average precipitation increases by 10%, the median value of the MMS is likely to increase by 15% to 30%. Meanwhile, under all three climatic conditions, $\varepsilon_p$ increases when the annual precipitation becomes larger. The reason for this is that larger precipitation can intensify the surface routing process and lead to a larger rainfall-runoff ratio. Similarly, $\varepsilon_p$ is generally higher in the wetter condition than the dry one when comparing the three climatic conditions.

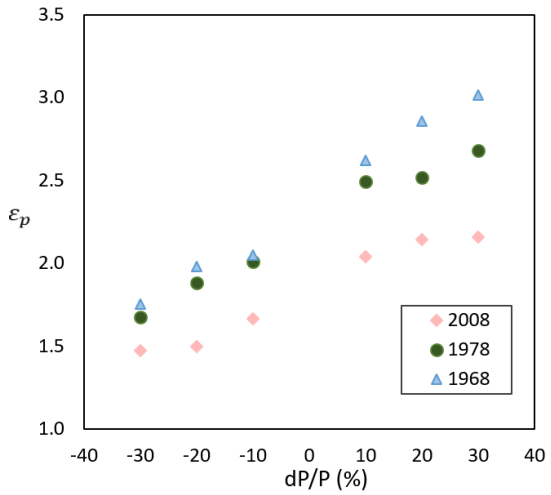


Figure 9 The results of the elasticity test under three kinds of climate conditions. The three conditions are: dry (2008, pink squares), normal (1978, green dots), and wet (1968, blue triangles).

In the second set, the elasticity of streamflow to precipitation was tested under three different land cover maps (Figure 10). The land cover maps were adopted from CLCS with three different urban conditions (i.e., ULC1986, ULC2000, ULC2011). The elasticity values range from 1.6 to 3.1. Compared with the results from the first set, the differences among the results of various urban conditions are small. This is because the range of the percent of the impervious area (from 4.9% in 1986 to 7.7% in 2011) is relatively smaller than the range from the precipitation (from 398mm in 2008 to 1025mm in 1968). This suggests that climate change has more significant effects on the MMS than urbanization. In the case of -30% observed precipitation, the elasticity for ULC2011 is much smaller than the elasticity for ULC1986 and ULC2000. One possible reason is that when the precipitation is very small, most of it becomes soil moisture and evapotranspiration, while little can reach the basin outlet in the form of runoff or base flow. Also, when there is more impervious area, DHSVM-Res is set up such that a higher portion of the surface runoff goes to the urban channel and thus the basin channel system.

Therefore, less surface runoff is available to go through the natural hydrological processes of infiltration and evaporation. Besides, in the case of -20% observed precipitation, the differences of the elasticity values from the three urban covers are very slight, which shows that the effect of urbanization to elasticity is relatively small under this precipitation condition. In the end, the elasticity results (-10%, 10%, - 20%, 20%, -30%, 30% precipitation) indicate that the largest elasticity using ULC2011 can be contributed to the increased impervious area.

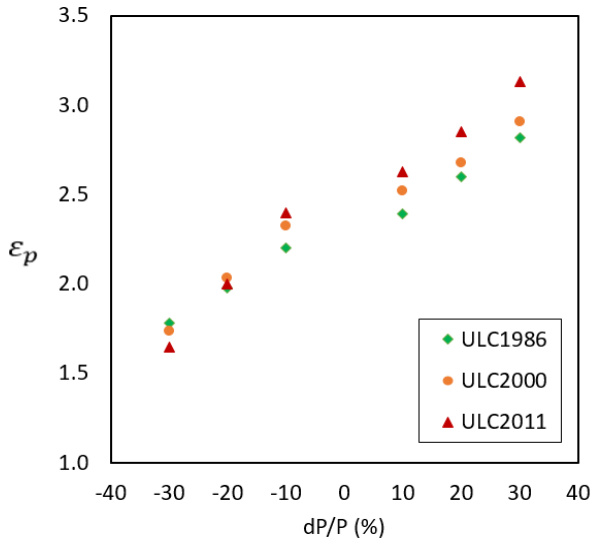


Figure 10 The results of the elasticity test under three urban land cover maps.

# 5. DISCUSSIONS

In this study, the individual and joint impacts of urbanization and climate change on streamflow were comprehensively investigated by leveraging the benefits from four aspects: paired catchments method, a distributed hydrological model, change point analysis method, and the precipitation elasticity test. As compared to previous studies which relied on available NLCD datasets (4 in total from 1992 to 2011) to represent the urbanization processes, our results are more realistic and representative by adopting the continuous annual urban land cover. Furthermore, the use of synthetic forcing series (with the interannual variation removed) allowed us to effectively separate out the urbanization and climate change effects on the peak flows. Considering there are almost a half of the world's population live in urban areas (United Nations 2014) and nearly 2.5 billion people reside in arid or semiarid regions (Reynolds et al. 2007), the results are representative and the approach is potentially applicable to other basins/watersheds. Specifically, more discussions are summarized as below:

1) The selection of the paired catchments depends on the climate similarity and the urbanization disparity, as our main objective is to separate the impacts from urbanization and climate change. This sets an example for other studies to choose paired catchments for similar purpose. It is worth noting that the idea of paired catchment can be applied to either adjacent or nonadjacent basins/watersheds, as long as the pair share similar characteristics in terms of soil, area, elevation range, slope, aspect, vegetation and climate patterns (Hornbeck et al. 1993; Brown et al. 2005; Prosdocimi et al. 2015; Cheng et al. 2017). In fact, many studies about ungauged river basins have developed approaches for identifying river basins with similar characteristics (Jha and Smakhtin 2008).

2) To isolate the impact of urbanization and climate change on peak streamflow, we designed two sets of model simulations to keep one factor static/controlled while the impact of the other factor can be extracted. The first had the land cover fixed over a period while the second was driven by synthetic forcing data (with inter-annual variability removed). This approach is straightforward, and it is applicable to studies with the similar objective that focus on impacts either from land use /land cover (LULC) changes (e.g., deforestation, desertification, and agricultural expansion) or from climate change/variability. In addition to the field of hydrology, this approach can also be employed to isolate the impacts of LULC changes on environmental and ecological terms such as eutrophication condition, aquatic biodiversity, and ecosystem health.

3) The CLCS facilitated the change point (CP) detection of the urban impervious area, because non-realistic CP is likely to be caused by the discrete data. Considering LULC has impact on energy balance and hydrological cycle (Zhu and Woodcock 2014), the use of continuous land cover maps is necessary for accurate hydrologic modeling and also for many land/water management purposes. Google Earth Engine (GEE; Gorelick 2017), on which our classification was conducted, is a free cloud-computing platform for geospatial analysis from local to global scale. The advantage of the distributed hydrological model can then be amplified by leveraging the computing power of GEE.

4) The elasticity test applied in this study using monthly maximum streamflow (MMS) is different from the traditional estimator (i.e., the average streamflow). There are two primary reasons: one is that urbanization primarily elevates peak flow (Rose and Peters 2001); the other one is that DHSVM-Res does not perform well with the base flow simulations. Elasticity results under three kinds of climate conditions (i.e.,

dry/normal/wet) were compared for the purpose of testing the streamflow sensitivity under different climate conditions in this region. The elasticity tests under the normal conditions are most relevant to the averaged future climate conditions. In contrast, the wet or dry conditions can be used for approximating the future extreme conditions, or quantify the streamflow uncertainties caused by the large uncertainties from different general circulation models (GCMs). Under a variety of perturbing synthetic forcing series for the SARB, the elasticity values range from 1.5 to 3.0. Hence, the elasticity results of our study can be used as a reference for other basins/watersheds in semi-arid/arid regions.

Even though our modeling framework can provide useful information for local water resources management, there are still three limitations worth noting. First, to keep the consistency in the generated CLCS, we only used the satellite images collected by Landsat 5 TM sensor from 1984 to 2011. The length of this study period can be extended to more recent years by incorporating images collected by Landsat 7 and 8. Using a longer period will stabilize the CP detection and can be more informative to current and near future water resources management. Second, the calibration and validation results (as shown in Figure 10) suggest that the capability of DHSVM-Res in base flow simulation is limited, which is caused by the lack of explicit hydrogeological simulation. This limitation can be alleviated by adding the observed spring discharge to the modeling framework. Third, the rescaling precipitation series generated by CDF mapping technique only reflect the change of the annual mean precipitation, and the impact of extreme event on streamflow was not fully investigated.

In the end, we plan to carry out some future extensions to this study. First, by incorporating newly collected satellite images, the study period can be extended to more

recent years. Second, elasticity simulations can be extended by including future climate sensitivity test, via the application of regional climate models (Feser et al. 2011) to make the results more informative for future policy making process. Third, the impact of historical extreme rainfall events on the streamflow under different urbanization progresses will be investigated. Fourth, multiple low impact development (LID) designs have been implemented in the City of San Antonio, considering the benefits such as storm water reduction and improved groundwater recharge. However, the effectiveness of different designs is still not fully understood especially in the hydrological regime. Our future work will involve evaluating the impacts of different LID designs such as permeable pavement and green roofs on the mitigation of flooding events.

# 6. CONCLUSIONS

The objective of this study is to systematically evaluate the impacts of urbanization and climate change on streamflow. First, a pair of adjacent basins with similar climate pattern, but distinct urbanization progresses were selected. Based on the Landsat images and the available NLCD land cover maps, CLCS for the San Antonio City Area were created from 1986 to 2011. With respect to precipitation, a number of synthetic forcing data series were generated based on the observed precipitation. Subsequently, the Distributed Hydrology Soil Vegetation Model (DHSVM) was employed to evaluate how urbanization and will impact the peak flows in the two neighboring basins both separately and jointly.

The five conclusions are summarized as follows:

1) The climate patterns of both basins are very similar with the same (change point) CPs detected in the precipitation time series.

2) The change of monthly peak flows (i.e., MMS) is mainly contributed by the changing precipitation when there is little or no urbanization, which is the case for the GRB.

3) The CP of the observed monthly maximum flow (i.e. MMS-Obs) for the SARB is mainly contributed by the urbanization process in the San Antonio City area.

4) The elasticity values of $\varepsilon_{P_n}$ range from 1.5 to 3.0 for the SARB and it is found that $\varepsilon_{P_n}$ increases when the annual precipitation becomes larger under all three climatic conditions.

5) Under three different land cover maps, the elasticity values of $\varepsilon_{P_n}$ range from 1.6 to 3.1 for the SARB. Specifically, the elasticity values of precipitation (-10%, 10%, -

20%, 20%, -30%, 30%) suggest that the larger elasticity can be contributed to the increased impervious area.

# REFERENCES


Anderson, B. T., Gianotti, D. J., and Salvucci, G.D. (2015). "Detectability of Historical Trends in Station-based Precipitation Characteristics over the Continental United States." *Journal of Geophysical Research: Atmospheres* 120: 4842–4859.

Asquith, W.H., Thompson, D.B., Cleveland, T.G. and Fang, X. (2004). "Synthesis of Rainfall and Runoff Data Used for Texas Department of Transportation Research Projects." Open-File Report 2004–1035.

Bates, C. G. and Henry, A. J. (1928). "Second Phase of Streamflow Experiment at Wagon Wheel Gap, Cold." *Monthly Weather Review* 56(3): 79–81.

Birge, L., Massart, P. (2007). "Minimal Penalties for Gaussian Model Selection." *Probability Theory and Related Fields* 138(1), 33–73.

Breiman, L. (2001). "Random Forests." *Machine Learning* 45: 5-32.

Brirhet, H. and Benaabidate, L. (2016). "Comparison of Two Hydrological Models (Lumped and Distributed) over a Pilot Area of the Issen Watershed in the Souss Basin, Morocco." *European Scientific Journal* 12(18): 347–358.

Brown, A.E., Zhang, L., McMahon, T.A., Western, A.W. and Vertessy, R.A. (2005). "A Review of Paired Catchment Studies for Determining Changes in Water Yield Resulting from Alterations in Vegetation." *Journal of Hydrology* 310(2005): 28–61.

Burns, D., Vitvar, T., McDonnell, J., Hassett, J. and Duncan, J. (2005). "Effects of Suburban Development on Runoff Generation in the Croton River Basin, New York, USA." *Journal of Hydrology* 311(1–4): 266–281.

Cao, Q., Sun, N., Yearsley, J., Nijssen, B. and Lettenmaier, D.P. (2016). "Climate and

Land Cover Effects on the Temperature of Puget Sound Streams." *Hydrological Processes* 30(13): 2286–2304.

Ellison, D., Dugan, J., Looney, C., Mendoza, J.G., Egan, K. et al. (2012). "San Antonio Demographic Distribution and Change: 2000 to 2010." Summary Report. Department of Planning and Community Development.

Chang, J., Wang, Y., Istanbulluoglu, E., Bai, T., Huang, Q. et al. (2015). "Impact of Climate Change and Human Activities on Runoff in the Weihe River Basin, China." *Quaternary International* 380-381(2015): 169–179.

Cheng, L., Zhang, L., Chiew, F.H.S, Canadell, J.G., Zhao, F. et al. (2017). "Quantifying the Impacts of Vegetation Changes on Catchment Storage – Discharge Dynamics Using Paired – catchment Data" *Water Resources Research* 53(7): 5963 – 5979.

Chu, H.J., Lin, Y.P., Huang, C.W., Hsu, C.Y. and Chen, H.Y. (2010). "Modelling the Hydrologic Effects of Dynamic Land-use Change Using a Distributed Hydrologic Model and a Spatial Land-use Allocation Model." *Hydrological Processes* 24(18): 2538–2554.

Stein, Robert (2018). "Hurricane Harvey: Experiences, Consequences and Public Support for Proposed Policies." Urban Flooding & Infrastructure Conference: Moving forward from Harvey, Conference 2018, Rice University, Houston, Texas.

Cuo, L., Lettenmaier, D. P., Mattheussen, B.V., Storck, P. and Wiley, M. (2008). "Hydrologic Prediction for Urban Watersheds with the Distributed Hydrology–Soil–Vegetation Model." *Hydrological Processes* 22: 4205–4213.

DeFries, R. and Eshleman, K. N. (2004). "Land-use Change and Hydrologic Processes: a Major Focus for the Future." *Hydrological Processes* 18(11): 2183–2186.

De Rosa, M., Knudsen, M. T. and Hermansen, J. E. (2016). "A Comparison of Land Use Change Models: Challenges and Future Developments." *Journal of Cleaner Production* 113: 183–193.

Daniel, P. L., Eugene, Z. S. and Lynn, R. M. (2000). "Sustainable Water Resources Management." *Journal of Water Resources Planning and Management* 126(2): 43–47.

Donges, K. (2018). "The Random Forest Algorithm" Access date: Jan 14th, 2018. Access link: https://machinelearning-blog.com/2018/02/06/the-random-forest-algorithm/#more-375

Du, J., Qian, L., Rui, H., Zuo, T., Zheng, D. et al. (2012). "Assessing the Effects of Urbanization on Annual Runoff and Flood Events Using an Integrated Hydrological Modeling System for Qinhuai River Basin, China." *Journal of Hydrology* 464–465: 127–139.

Du, P., Samat, A., Waske, B., Liu, S. and Li, Z. (2015). "Random Forest and Rotation Forest for Fully Polarized SAR Image Classification Using Polarimetric and Spatial Features." *ISPRS Journal of Photogrammetry and Remote Sensing* 105: 38–53.

Eric, S.B. and Zelinsky, D.A. (2018). "National Hurricane Center Tropical Cyclone Report: Hurricane Harvey." National Hurricane Center.

Fang, X., Thompson, D.B., Cleveland, T.G. and Pradhan, P. (2007). "Variations of Time of Concentration Estimates Using NRCS Velocity Method." *Journal of Irrigation and Drainage Engineering* 133(4): 314–322.

Rodriguez, F., Andrieu, H. and Morena, F. (2008). "A Distributed Hydrological Model

for Urbanized Areas – Model Development and Application to Case Studies." *Journal of Hydrology* 351(2008): 268–287.

Feser, F., Rockel, B., Storch, H., Winterfeldt, J. and Zahn, M. (2011). "Regional Climate Models Add Value to Global Model Data: a Review and Selected Examples." *American Meteorological Society* 92: 1181–1192.

Fletcher, T.D., Andrieu, H. and Hamel, P. (2013). "Understanding, Management and Modelling of Urban Hydrology and Its Consequences for Receiving Waters: A State of the Art". *Advances in Water Resources* 51: 261–279

Frans, C., Istanbulluoglu, E., Lettenmaier, D.P., Clarke, G., Bohn, T.J. et al. (2016). "Implications of Decadal to Century Scale Glacio-hydrological Change for Water Resources of the Hood River Basin, OR, USA." *Hydrological Processes* 30: 4314–4329.

Fry, J. A., Xian, G., Jin, S., Dewitz, J., Homer, C. et al. (2011). "Completion of the 2006 National Land Cover Database for the Conterminous United States." *Photogrammetric Engineering and Remote Sensing* 77(9): 858–864.

Gorelick, N., Hancher, M., Dixon, M., Ilyushchenko, S., Thau, D. et al. (2017). "Google Earth Engine: Planetary-scale Geospatial Analysis for Everyone." *Remote Sensing of Environment.* 202: 18–27.

Killick, R. and Eckley, I. A. (2014). "Changepoint: An R Package for Changepoint Analysis." *Journal of Statistical Software* 58(3): 1–19.

Guannel, G., Guerry, A., Brenner, J., Faries, J., Thompson, M. et al. (2014). "Changes in the Delivery of Ecosystem Services in Galveston Bay, TX, Under a Sea-Level Rise Scenario." The Nature Conservancy.

Homer, C., Dewitz, J., Fry, J., Coan, M., Hossain, N. et al. (2007). "Completion of the 2001 National Land Cover Database for the Conterminous United States." *Photogrammetric Engineering and Remote Sensing* 73: 337–341.

Hornbeck, J.W., Adams, M.B., Corbett, E.S., Verry, E.S. and Lynch, J.A. (1993). "Long-term Impacts of Forest Treatments on Water Yield: A Summary for Northeastern USA." *Journal of Hydrology* 150: 323–344.

Jarvis, A., Reuter, H. I., Nelson, A. and Guevara, E. (2008). "Hole-Filled SRTM for the Globe Version 4." CGIAR-CSI SRTM 90m Database. Access date: December 12th, 2016. Access link: http://srtm.csi.cgiar.org.

Jin, S., Yang, L., Danielson, P., Homer, C., Fry, J. et al. (2013). "A Comprehensive Change Detection Method for Updating the National Land Cover Database to Circa 2011." *Remote Sensing of Environment* 132: 159–175.

Jha, A. K., Bloch, R. and Lamond, J. (2012). "Cities and Flooding: A Guide to Integrated Urban Flood Risk Management for the 21st Century." Washington DC, The World Bank.

Jha, R. and Smakhtin, V. (2008). "A Review of Methods of Hydrological Estimation at Ungauged Sites in India." Colombo, Sri Lanka: International Water Management Institute (IWMI). 18p. (IWMI Working Paper 130)

Jog, S. and Dixit, M. (2016). "Supervised Classification of Satellite Images." Conference on Advances in Signal Processing (CASP). Pune, India.

JR, J. C.M and Tucci, C. E. M. (1984). "Simulation of the Urbanization Effect in Flow." *Hydrological Sciences Journal* 29(2): 131–147.

Krause, P., Boyle, D.P., and Baese, F. (2005). "Comparison of Different Efficiency

Criteria for Hydrological Model Assessment." *Advances in Geosciences* 5: 89–97.

Lee, J. G. and Heaney, J.P. (2003). "Estimation of Urban Imperviousness and Its Impacts on Storm Water Systems." *Journal of Water Resources Planning and Management* 129(5): 419–426.

Lindner, J. (2018). "Hurricane Harvey." Urban Flooding & Infrastructure Conference: Moving forward from Harvey. Rice University, Houston, Texas.

Lin, Y.P., Hong, N.M., Wu, P.J., Wu, C.F. and Verburg, P.H. (2007). "Impacts of Land Use Change Scenarios on Hydrology and Land Use Patterns in the Wu–Tu Watershed in Northern Taiwan." *Landscape and Urban Planning* 80 (1–2): 111–126.

Livneh, B., Rosenberg, E. A., Lin, C., Nijssen, B., Mishra, V. et al. (2013). "A Long-Term Hydrologically Based Dataset of Land Surface Fluxes and States for the Conterminous United States: Update and Extensions." *Journal of Climate* 26(23): 9384–9392.

Maclay, R.W and Land, L.F. (1988). "Simulation of Flow in the Edwards Aquifer, San Antonio Region, Texas, and Refinement of Storage and Flow Concepts." Chapter A of USGS water-supply paper.

Marshall, E., and Randhir, T.O. (2008). "Spatial Modeling of Land Cover Change and Watershed Response Using Markovian Cellular Automata and Simulation." *Water Resources Research* 44(4): 1–11.

Nash, J.E and Sutcliffe, J. V. (1970). "River Flow Forecasting Through Conceptual Models Part I—A discussion of Principles." *Journal of Hydrology* 10(3): 282–290.

Natkhin, M., Dietrich, O., Schäfer, M.P. and Lischeid, G. (2013). "Quantifying the Effect of Climate and Changing Land Use on the Discharge Regime of a Small Catchment in Tanzania." *Regional Environmental Change* 15(7): 1269–1280.

National Weather Service. (2018). "Advanced Hydrologic Prediction Service." National Oceanic and Atmospheric Administration.

Nauman, R., Dangermond, M. and Frye, C. (2018). "Soil Survey Geographic (SSURGO) Database for Texas." United States Department of Agriculture. Access date: December 12th, 2016. Access link: https://www.nrcs.usda.gov/wps/portal/nrcs/detail/soils/survey/geo/?cid=nrcs142p2_053631

Nowak, D. J. and Greenfield, E. J. (2012). "Tree and Impervious Cover in the United States." *Landscape and Urban Planning* 107(1): 21–30.

Ogden, F.L., Pradhan, N.R., Downer, C.W. and Zahner, J.A. (2011). "Relative Importance of Impervious Area, Drainage Density, Width Function, and Subsurface Storm Drainage on Flood Runoff from an Urbanized Catchment." *Water Resources Research* 47(12): 1–12.

Oni, S.K., Futter, M.N., Buttle, J. and Dillon, P. J. (2015). "Hydrological Footprints of Urban Developments in the Lake Simcoe Watershed, Canada: A Combined Paired-catchment and Change Detection Modelling Approach." *Hydrological Processes* 29(7): 1829–1843.

Pal, M. (2005). "Random Forest Classifier for Remote Sensing Classification." *International Journal of Remote Sensing* 26(1): 217–222.

Phiri, D. and Morgenroth, J. (2017). "Developments in Landsat Land Cover

Classification Methods: A Review." *Remote Sensing* 9(967): 1–25

Price, C.V., Nakagaki, N., Hitt, K.J. and Clawges, R.C. (2006). "Enhanced Historical Land-Use and Land-Cover Data Sets of the U.S. Geological Survey." U.S. Geological Survey Digital Data Series 240. Access date: 16th April 2017. Access link: https://water.usgs.gov/GIS/metadata/usgswrd/XML/ds240_landuse_poly.xml.

Prosdocimi, I., Kjeldsen, T. R. and Miller, J. D. (2015). "Detection and Attribution of Urbanization Effect on Flood Extremes Using Nonstationary Flood-frequency Models." *Water Resources Research* 51(7): 4244–4262.

Reynolds, J.F., Smith, D.M.S., Lambin, E.F. et al. (2007). "Global Desertification: Building a Science for Dryland Development." *Science* 316(5826): 847–851.

Rose, S. and Peters, N.E. (2001). "Effects of Urbanization on Streamflow in the Atlanta Area (Georgia, USA): A Comparative Hydrological Approach." *Hydrological Processes* 15: 1441–1457.

Spence, M., Annez, P.C. and Buckley, R.M. (2008). "Urbanization and Growth." The World Bank.

Shelestov, A., Lavreniuk, M., Kussul, N., Novikov, A. and Skakun, S. (2017). "Exploring Google Earth Engine Platform for Big Data Processing: Classification of Multi-Temporal Satellite Imagery for Crop Mapping." *Frontiers in Earth Science* 5 (17): 1–7.

Sankarasubramanian, A., Vogel, R.M. and Limbrunner, J.F (2001). "Climate Elasticity of Streamflow in the United States." *Water Resources Research*, 37(6):1771-1781.

Schaake, J. C. (1990). "From Climate to Flow." *Climate Change and U.S. Water*

*Resources*: 177–206.

Texas Water Development Board (TWDB). (2001). "Volumetric Survey of Canyon Lake." Access date: March 5th 2018. Access link: https://www.twdb.texas.gov/hydro_survey/Canyon/2001-11/Canyon2000_FinalReport.pdf.

Texas Water Development Board (TWDB). (2018). "Water Data for Texas." Access date: March 5th 2018. Access link: https://waterdatafortexas.org/reservoirs/individual/canyon.

Texas Water Development Board (TWDB). (2018). "Texas Water Conditions and Data." Access date: March 5th 2018. Access link: https://www.twdb.texas.gov/surfacewater/conditions/index.asp

Thomas, L. M., Nancy, A. P., Enrique, J. L. and Enrique, J. L. (2013). "U.S. Census Bureau 2010 Census of Population and Housing, Summary Population and Housing Characteristics." U.S. Census Bureau.

Turok, I. and McGranahan, G. (2013). "Urbanization and Economic Growth: The Arguments and Evidence for Africa and Asia." *Environment and Urbanization* 25(2): 465–482.

United Nations (2014). "World Urbanization Prospects: The 2014 Revision."

U.S. Geological Survey (USGS). (2014). "Floods in the Guadalupe and San Antonio River Basins in Texas, October 1998." Access date: April 5th 2017. Access link: https://pubs.usgs.gov/fs/FS-147-99/

U.S. Geological Survey (USGS). (2016). "National Water Information System data

available on the World Wide Web (USGS Water Data for the Nation).” Access date: Jan 10th, 2018. Access link: http://waterdata.usgs.gov/nwis/

U.S Army Corps of Engineers (USACE). (2017) “Canyon Lake.” Access date: April 5th 2017. Access link: http://www.swf-wc.usace.army.mil/canyon/

Vogelmann, J. E., Howard, S. M., Yang, L., Larson, C.R., Wylie, B.K. et al. (2001). “Completion of the 1990s National Land Cover Data Set for the Conterminous United States from Landsat Thematic Mapper Data and Ancillary Data Sources.” *Photogrammetric Engineering and Remote Sensing* 67: 652-662.

Wasko, C. and Sharma, A. (2017). “Global Assessment of Flood and Storm Extremes with increased temperatures.” *Scientific Reports*: 7–7945

Weinmann, M., Schmidt, A., Mallet, C. et al. (2015). “Contextual Classification of Point Cloud Data by Exploiting Individual 3D Neighborhoods.” *ISPRS Annals of Photogrammetry, Remote Sensing and Spatial Information Sciences* 2(3–W4).

Wigmosta, M.S., Vail, L.W. and Lettenmaier, D.P. (1994). “A Distributed Hydrology-Vegetation Model for Complex Terrain.” *Water Resources Research* 30(6): 1665–1679.

Winters, B. A., Angel, J., Ballerine, C., Byard, J., Flegel A. et al. (2015). “Report for the Urban Flooding Awareness Act.” Illinois Department of Natural Resources. Access date: April 10th, 2018. Access link : https://www.dnr.illinois.gov/WaterResources/Documents/Final_UFAA_Report.pdf

Yang, L., Smith, J.A., Wright, D.B., Baeck, M.L., Villarini G. et al. (2013).

"Urbanization and Climate Change: An Examination of Nonstationarities in Urban Flooding." *Journal of Hydrometeorology* 14: 1791–1809.

Yang, L., Feng, Q., Yin, Z., Deo, R.C., Wen, X. et al. (2017). "Separation of the Climatic and Land Cover Impacts on the Flow Regime Changes in Two Watersheds of Northeastern Tibetan Plateau." *Advances in Meteorology* 2017: 1–15.

Zhao, G., Gao, H. and Cuo, L. (2016). "Effects of Urbanization and Climate Change on Peak Flows over the San Antonio River Basin, Texas." *Journal of Hydrometeorology* 17(9): 2371-2389

Zhao, G., Gao, H., Naz, B.S., Kao, S-C. and Voisin, N. (2016). "Integrating a Reservoir Regulation Scheme into a Spatially Distributed Hydrological Model." *Advances in Water Resources* 98: 16–31.

Zarezadeh, V., and Giacomoni, M. (2017). "Incorporating Dynamic Land Use Change into Hydrologic Model to Assess Urbanization Effects on Hydrologic Flow Regime." *World Environmental and Water Resources Congress*: 22–32.

Duan, Z. (2017). GitHub repository. Access date: Jan 5th 2018. Access link: https://github.com/pnnl/DHSVMPNNL/tree/master/CreateStreamNetwork_PythonV

Zhu, Z. and Woodcock, C.E. (2014). "Continuous Change Detection and Classification of Land Cover Using All Available Landsat Data." *Remote Sensing of Environment* 144: 152–171.

Zhu, Z., Wang, S. and Woodcock, C.E. (2015). "Improvement and Expansion of the Fmask Algorithm: Cloud, Cloud Shadow, and Snow Detection for Landsats 4–7, 8, and Sentinel 2 images." *Remote Sensing of Environment* 159 (2015): 269–277.

# APPENDIX A

The soil texture of the study area are shown in Figure A-1. The main soil type in the study area is clay.

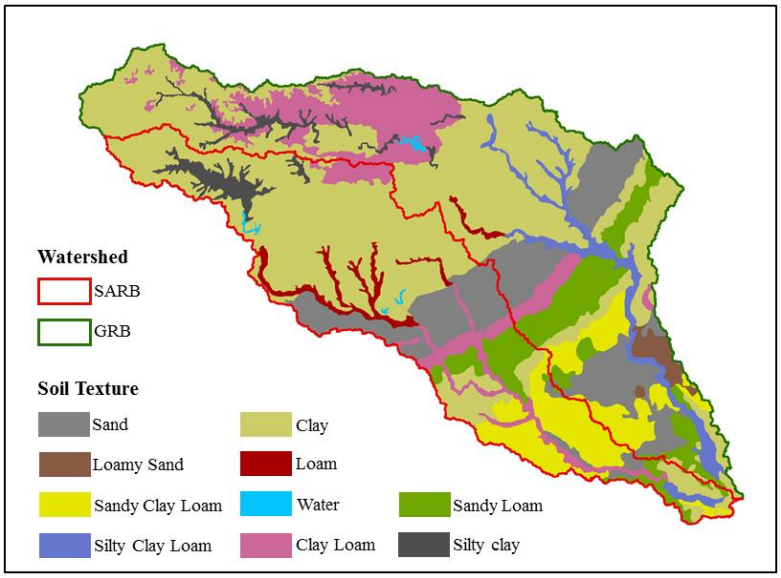


Figure A-1. Soil Texture Maps for the GRB and the SARB

# APPENDIX B

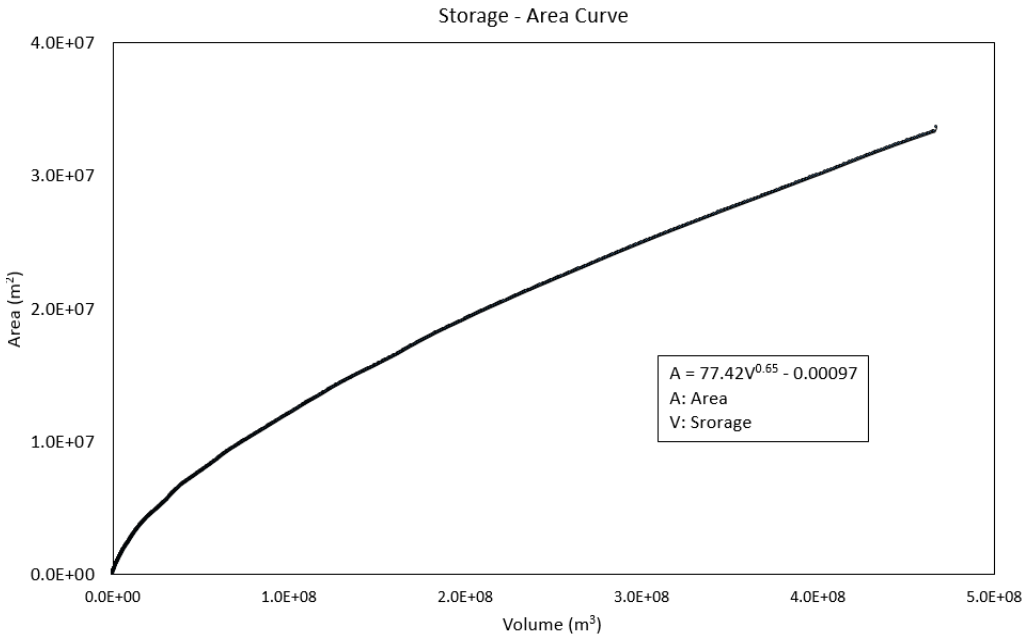


Figure B-1. The fitted storage – area curve for the Canyon Lake in the GRB.

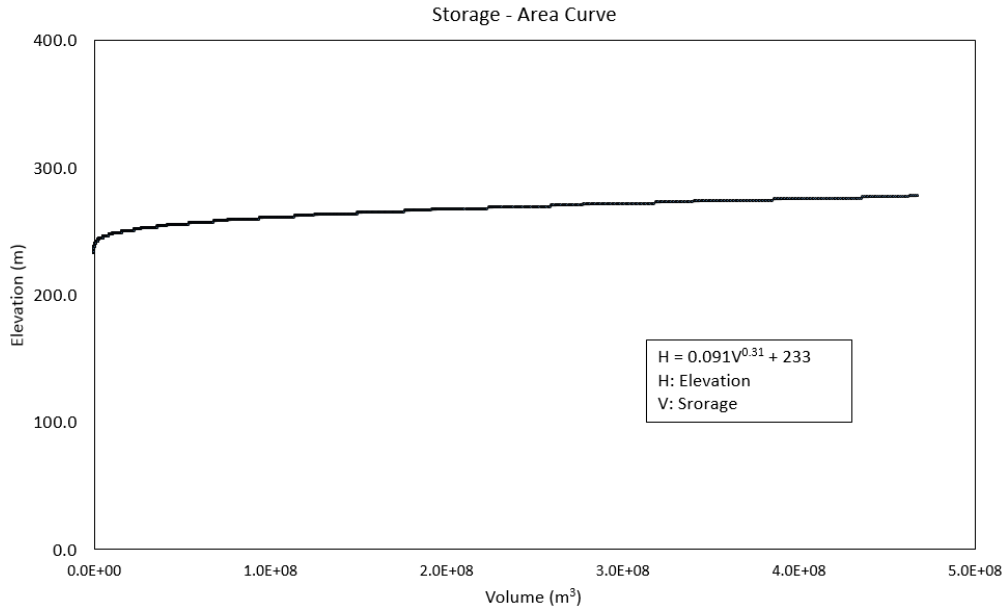


Figure B-2. The fitted storage – elevation curve for the Canyon Lake in the GRB.

# APPENDIX C

Fang et al. (2007) compared the time of concentration (*Tc*) results over 96 Texas watersheds, with the *Tc* estimated using the Natural Resources Conservation Service (NRCS) velocity method by three research teams. Fang et al. (2007) also compare the results with Eq. (C-1):

$$T_c = 0.62\ A^{0.5} \qquad \text{Eq. (C-1)}$$

$T_c =$ Time of concentration for the watershed

$A =$ Area of the watershed

Because there are many uncertainties when calculating the time of concentration, Fang et al. (2007) suggested that the above equation can be used as a general method for cross-validating other methods or for calculating $T_c$ when data are limited.

Asquith et al. (2004) studied the watersheds in several large cities of Texas (e.g., Austin, Dallas) including the City of San Antonio, but not in the GRB, for the purpose to estimate $T_c$. Hence, we focus the SARB and divided the whole drainage area of the SARB to a number of small watersheds with the same area based on a representative area (119 $km^2$). The representative area was calculated by comparing all the areas of the 96 watersheds (Fang et al. 2007).

The drainage area of USGS 08188500 (the SARB) is 10155 $km^2$. Then the $T_c$ for the whole SARB was estimated by adding all the Tc of the representative area. In the end, the $T_c$ of the whole SABR was estimated as 576 hours (24 days). Because the SARB and the GRB have similar topography and climate. The $T_c$ is considered to be the same for both basins for the convenience of analysis.